JOURNAL OF COMPUTATIONAL PHYSICS **123,** 435–449 (1996)
ARTICLE NO. 0035

On the Stability of Godunov-Projection Methods for Incompressible Flow[1]

MICHAEL L. MINION

Courant Institute of Mathematical Sciences, New York University, 251 Mercer Street, New York, New York 10012

Received April 3, 1995; revised October 1995

An analysis of the stability of certain numerical methods for the linear advection–diffusion equation in two dimensions is performed. The advection–diffusion equation is studied because it is a linearized version of the Navier–Stokes equations, the evolution equation for density in Boussinesq flows, and a simplified form of the equations for bulk thermodynamic temperature and mass fraction in reacting flows. It is found that various methods currently in use which are based on a Crank–Nicholson type temporal discretization utilizing second-order Godunov methods for explicitly calculating advective terms suffer from a time-step restriction which depends on the coefficients of diffusive terms. A simple modification in the computation of the advective derivatives results in a method with a stability condition that is independent of the magnitude of the coefficients of the diffusive terms. © 1996 Academic Press, Inc.

CONTENTS

1. INTRODUCTION

This paper is intended to clarify the CFL condition necessary for the stability of various versions of the second-order Godunov/projection method for two-dimensional, incompressible flow first proposed by Bell, Colella, and Glaz (BCG) [2]. This method is a second-order extension of the projection method introduced by Chorin [8, 7, 9]. (For a survey of projection methods, see Peyret and Taylor [16], Gresho [12], or Simo [18].)

Since the introduction of the basic method for viscous flows, variations of and extensions to the BCG method have been proposed for an increasingly wide range of problems including variable density flow [4], reacting flow in the zero Mach number limit [13], and incompressible flow on locally refined meshes [1, 15]. In each of the above papers, the claim is made that the condition for stability of the overall method is essentially the advective CFL condition

$$u\Delta t/h \le 1 \quad \text{and} \quad v\Delta t/h \le 1, \tag{1}$$

where u and v are the horizontal and vertical velocity components and h is the grid spacing. This condition is used regardless of the magnitude of the viscosity.

The BCG method has been shown to stably compute viscous, constant density flows under condition (1) for a variety of problems. (See any of the works cited above for examples.) However, the analysis of the linearized equations given below will show this condition is not sufficient for the extensions of the method to flows with density variations currently in use, and an example is provided that shows the method can give unstable results for a nonlinear constant density problem as well. A simple, inexpensive modification to the BCG method will be introduced that results in a method that is stable for the linearized problem under condition (1) regardless of the size of viscous terms.

The simplest form of incompressible flow which is coupled with a density equation is the so-called Boussinesq approximation given by the following equations. (See Chandrasekhar [6] for a derivation of the Boussinesq approximation.) Let $U = (u, v)^{\mathrm{T}}$ denote the two-dimensional fluid velocity, p the pressure, ρ the density, ν the fluid viscosity, κ the diffusivity, and γ the gravitational constant. Then

$$\begin{aligned} U_t &= -(U\cdot\nabla)U - \nabla p + \nu\Delta U + \gamma\hat{\mathbf{j}}\rho \\ \rho_t &= -(U\cdot\nabla)\rho + \kappa\Delta\rho \\ \nabla\cdot U &= 0. \end{aligned} \tag{2}$$

In the original BCG method for constant density flow, the first equation above is discretized using the second-order,

[1] This work made possible by a grant from the U.S. Department of Energy under Contract DE-FG02-92ER25139. Calculations were performed at Los Alamos National Lab under Contract W-7405-ENG-36.

0021-9991/96 $18.00
Copyright © 1996 by Academic Press, Inc.
All rights of reproduction in any form reserved.

Crank–Nicholson type formulation (omitting the gravity term)

$$\frac{U^{n+1}-U^n}{\Delta t}+\nabla p^{n+1/2} = -[(U\cdot\nabla)U]^{n+1/2}+\frac{\nu}{2}\Delta(U^n+U^{n+1}), \tag{3}$$

where the term $[(U\cdot\nabla)U]^{n+1/2}$ is calculated explicitly using a second-order Godunov procedure. Subsequent extensions to the BCG method for Boussinesq and variable density flows [4] use an analogous formulation for the density equation. Also, extensions to reacting flows [13] use this form for the equations for temperature and mass fraction. In Section 2, it will be shown using a Von Neumann analysis that this treatment of the density equation has a stability condition that depends on the magnitude of κ despite the use of the Crank–Nicholson discretization for the temporal derivatives.

In Section 3 a slight modification to the BCG method is presented that removes the dependence of the stability restriction on κ and, hence, recovers the stability condition (1) when the method is applied to the linearized form of the density equation above. Since this is also the linearized form of the Navier–Stokes equations and the modification to the scheme requires very little extra computation compared to the BCG method, the modification should be used for the treatment of the velocity equations also. The analysis presented in Section 4 of a special oscillating flow that is unstably treated by the original BCG method gives further justification for applying the modification to the nonlinear problem. In Section 5, numerical experiments illustrating the instability of the original BCG method are presented as well as experiments showing the stabilizing effect of the modification presented in Section 3.

2. STABILITY OF THE BCG METHOD

In order to illustrate the stability requirements of the full BCG method for the Boussinesq equations, the simplified case of constant velocity and zero gravity will be considered. This reduces Eqs. (2) to the linear advection–diffusion equation

$$\rho_t = -a\rho_x - b\rho_y + \kappa\Delta\rho, \tag{4}$$

where a and b are assumed positive constants. As in Eq. (3), the method for approximating Eq. 4 that will be considered is based on the discretization

$$\frac{\rho^{n+1}-\rho^n}{\Delta t} = -(a\rho_x+b\rho_y)^{n+1/2}+\frac{\kappa}{2}\Delta(\rho^n+\rho^{n+1}), \tag{5}$$

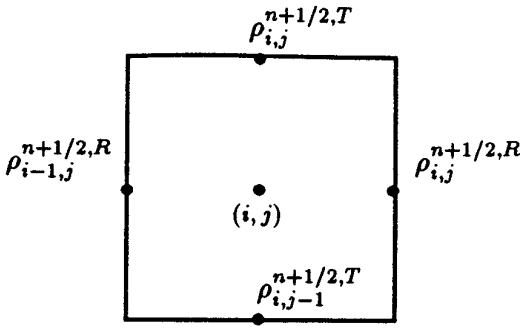

FIG. 1. Location of time-centered edge values.

where again the term $(a\rho_x + b\rho_y)^{n+1/2}$ is explicitly calculated using a second-order Godunov procedure. A Von Neumann analysis will be carried out on the method outlined by Eq. (5). For more complete details and motivations for the methods, the reader is asked to see [2] for the basic method or the works cited above for extensions.

The Godunov method for calculating the time-centered advective term in Eq. (5) proceeds by constructing time-centered, cell-edge values of ρ which are then differenced to yield the derivatives. (See Fig. 1 for variable locations.) Taylor series extrapolation to cell edges from cell-centered values is performed in which temporal derivatives are replaced by spatial derivatives using the equations of motion. This procedure results in two time-centered values at each cell edge, one computed by the Taylor series extrapolation from each adjacent cell center. In the nonlinear method, an upwinding procedure is employed to select which of these two values is used in the computation of the derivatives. Since both velocities are assumed to be positive in the linear case, the upwinding procedure has the effect of making the advective derivatives backward differences of the time-centered values $\rho^{n+1/2,T}$ and $\rho^{n+1/2,R}$ defined below. For example, the first order terms in the Taylor series expansion from cell centers to the top and right side cell edges have the form

$$\begin{aligned}\rho^{n+1/2,T} &= \rho^n+\frac{h}{2}\rho_y^n+\frac{\Delta t}{2}(-a\rho_x^n-b\rho_y^n+\kappa\Delta\rho^n)\\ \rho^{n+1/2,R} &= \rho^n+\frac{h}{2}\rho_x^n+\frac{\Delta t}{2}(-a\rho_x^n-b\rho_y^n+\kappa\Delta\rho^n).\end{aligned} \tag{6}$$

The following difference operators are used to approximate this Taylor series. Let D_x^- and D_y^- denote the backward differences in the x and y direction. For example

$$D_x^-(\rho)_{i,j} = \rho_{i,j}-\rho_{i-1,j}.$$

Likewise, let D_x^0 and D_y^0 denote centered differences in the x and y directions (e.g., $D_x^0(\rho)_{i,j} = (\rho_{i+1,j}-\rho_{i-1,j})/2$). Finally

let L^5 denote the standard five-point discrete Laplacian $L^5(\rho)_{i,j} = (D_x^+ D_x^-(\rho)_{i,j} + D_y^+ D_y^-(\rho)_{i,j})/h^2$.

The version of the Godunov method considered first is used in [13, 4], where derivative terms in Eq. (6) that are normal to a cell edge are replaced with centered differences, transverse derivative terms with upwind differences, and the diffusive terms with the standard five-point Laplacian operator. Using the above notation this gives

$$\begin{aligned}\rho_{i,j}^{n+1/2,T} &= \rho_{i,j} + \frac{1}{2}\left(1 - \frac{\Delta t}{h} b\right) D_y^0(\rho^n)_{i,j} - \frac{a\Delta t}{2h} D_x^-(\rho^n)_{i,j} \\ &\quad + \frac{\kappa \Delta t}{2} L^5(\rho^n)_{i,j}, \\ \rho_{i,j}^{n1/2,R} &= \rho_{i,j}^n + \frac{1}{2}\left(1 - \frac{\Delta t}{h} a\right) D_x^0(\rho^n)_{i,j} - \frac{b\Delta t}{2h} D_y^-(\rho^n)_{i,j} \\ &\quad + \frac{\kappa \Delta t}{2} L^5(\rho^n)_{i,j}.\end{aligned} \tag{7}$$

This will hereafter be referred to as the "base" method. The original BCG algorithm uses a slightly more complex form of the transverse derivative terms, and this is discussed at the end of this section and in Section 3. Also, in the actual implementation of BCG type methods, slope limiters similar to those developed by Van Leer [19] are applied to normal derivative terms, but in the following analysis the effect of limiters is not included.

The form of the time-centered advective derivative of ρ is now given by (suppressing the $n + 1/2$ superscripts)

$$\begin{aligned}(a\rho_x + b\rho_y)_{i,j} &= a\frac{(\rho_{i,j}^R - \rho_{i-1,j}^R)}{h} + b\frac{(\rho_{i,j}^T - \rho_{i,j-1}^T)}{h} \\ &= \frac{a}{h} D_x^-(\rho^R)_{i,j} + \frac{b}{h} D_y^-(\rho^T)_{i,j}.\end{aligned} \tag{8}$$

Now suppose that the function ρ is doubly-periodic on the region $[2\pi \times 2\pi]$ and write ρ as its discrete Fourier series

$$\rho_{i,j} = \sum_{k=-N/2}^{N/2-1} \sum_{l=-N/2}^{N/2-1} \hat{\rho}_{k,l} e^{\mathbf{i}(i\xi + j\eta)},$$

where $\xi = kh$ and $\eta = lh$. (The range of each is $[-\pi, \pi)$.)

Let μ and ϑ denote the Courant numbers $\mu = a\Delta t/h$ and $\vartheta = b\Delta t/h$, and define $\sigma = \kappa \Delta t/h^2$. A straightforward substitution of the spectral form of each of the difference operators used in the above equations results in the following symbol for one step of the base method:

$$\begin{aligned}\hat{\rho}_{k,l}^{n+1} &= S(\xi, \eta)\hat{\rho}_{k,l}^n \\ S(\xi, \eta) &= \Bigg[1 - \mu(1 - e^{-\mathbf{i}\xi}) \\ &\quad [1 + \frac{1}{2}(1 - \mu)\mathbf{i}\sin(\xi) - \frac{\vartheta}{2}(1 - e^{-\mathbf{i}\eta})] \\ &\quad - \vartheta(1 - e^{-\mathbf{i}\eta}) \\ &\quad \times [1 + \frac{1}{2}(1 - \vartheta)\mathbf{i}\sin(\eta) - \frac{\mu}{2}(1 - e^{-\mathbf{i}\xi})] \\ &\quad + \frac{\sigma}{2}[1 - \mu(1 - e^{-\mathbf{i}\xi}) - \vartheta(1 - e^{-\mathbf{i}\eta})] \\ &\quad \times (-4 + 2\cos(\xi) + 2\cos(\eta))\Bigg] \Bigg/ \\ &\quad \left[1 - \frac{\sigma}{2}(-4 + 2\cos(\xi) + 2\cos(\eta))\right].\end{aligned} \tag{9}$$

For the numerical method to be stable for given values of μ, ϑ, and σ, the maximum magnitude of $S(\xi, \eta)$ must be less than or equal to one for all values of ξ and η in the range $[-\pi, \pi]$. Let $\overline{S}(\mu, \vartheta, \sigma)$ be defined as the maximum value of $|S(\xi, \eta)|$ for the values μ, ϑ, σ. From Eq. (9), it is apparent that $S(0, 0) = 1$, hence $\overline{S}(\mu, \vartheta, \sigma) \geq 1$ for any μ, ϑ, and σ. The stability region for the numerical scheme is, hence, the region of space in which $\overline{S}(\mu, \vartheta, \sigma) = 1$.

As a simplest case, consider the one-dimensional flow when $b = 0$ and, hence, $\vartheta = 0$. In this case

$$\begin{aligned}S(\xi, \eta) &= [1 - \mu(1 - e^{-\mathbf{i}\xi})\Bigg[1 + \frac{1}{2}(1 - \mu)\mathbf{i}\sin(\xi)] \\ &\quad + \frac{\sigma}{2}[1 - \mu(1 - e^{-\mathbf{i}\xi})] \\ &\quad \times (-4 + 2\cos(\xi) + 2\cos(\eta))\Bigg] \Bigg/ \\ &\quad \left[1 - \frac{\sigma}{2}(-4 + 2\cos(\xi) + 2\cos(\eta))\right].\end{aligned}$$

Again, if the scheme is to be stable, $|S(\xi, \eta)| \leq 1$ for any ξ and η, so consider $S(\pi, \pi)$

$$\begin{aligned}S(\pi, \pi) &= (1 - 2\mu - 4\sigma + 8\mu\sigma)/(1 + 4\sigma) \\ &= (1 - 2\mu)\frac{1 - 4\sigma}{1 + 4\sigma}.\end{aligned}$$

Obviously it is necessary that $\mu \leq 1$ for stability, and it is only slightly more complicated to see that $\mu \leq 1$ assures

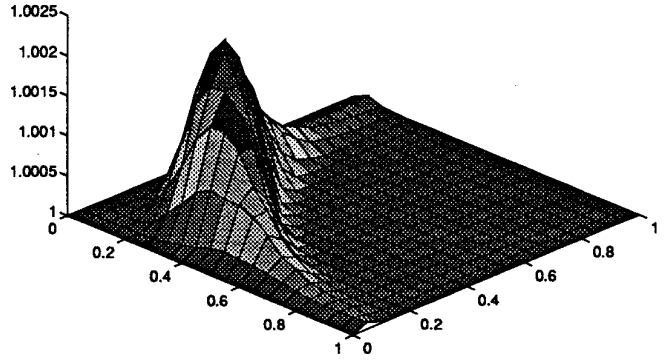

FIG. 2. Stability region for method when $\sigma = 0$ and fourth-order slopes are used. The axis in the plane corresponds to μ and ϑ, the verical axis is the magnitude of the symbol.

that the one-dimensional base method is stable for all values of σ.

For two-dimensional flow, the same procedure yields

$$\begin{aligned} S(\pi,\pi) &= (1-2\mu(1-\vartheta)-2\vartheta(1-\mu) \\ &\quad -4\sigma+8(\mu+\vartheta)\sigma)/(1+4\sigma) \\ &= ((1-2\mu)(1-2\vartheta)-4\sigma \\ &\quad +8\sigma(\mu+\vartheta))/(1+4\sigma). \end{aligned} \tag{10}$$

For $\sigma = 0$, $S(\pi, \pi)$ takes the familiar form $S(\pi, \pi) = (1 - 2\mu)(1 - 2\vartheta)$ which gives the stability condition (equivalent to condition (1))

$$\mu \le 1 \quad \text{and} \quad \vartheta \le 1. \tag{11}$$

A simple program to numerically check the symbol indicates that this condition is sufficient to stably treat all wave numbers when $\sigma = 0$.

If fourth-order limited slopes are used for the normal derivatives instead of second order as is often done in practice [13, 15, 3], the same numerical process indicates that, although the highest mode is stably treated under the condition (11), because of the appearance of terms with frequency 2ξ and 2η in the symbol, not all modes are. A numerically computed surface plot of $\overline{S}(\mu, \vartheta)$ is shown in Fig. 2. This figure is constructed by sampling μ and ϑ in the range [0, 1] at intervals of 1/20 and for each μ,ϑ pair computing the maximum of $|S(\xi, \eta)|$ over a range of values of ξ and η. By symmetry, only values of ξ and η in the range $[0, \pi]$ need to be sampled, and for the figures shown each were sampled at intervals of $\pi/20$.

Again consider (10). It is evident that for any value of σ greater than zero, using $\mu = \vartheta = 1$ will yield

$$S(\pi, \pi) = (1 + 12\sigma)/(1 + 4\sigma). \tag{12}$$

This quantity is always greater than one if $\sigma > 0$; hence, the base scheme is never stable with $\mu = \vartheta = 1$ and $\sigma > 0$. Since the symbol is continuous, the unstable region must contain some of the region given by (11); how much of this region of course depends on the size of σ. For example, $\sigma = \frac{1}{4}$ gives

$$\begin{aligned} S(\pi,\pi) &= ((1-2\mu)(1-2\vartheta)-1+2\mu+2\vartheta)/2 \\ &= 2\mu\vartheta. \end{aligned}$$

This indicates that a necessary stability condition is that $\mu\vartheta \le \frac{1}{2}$. A numerical check of the full symbol with $\sigma = \frac{1}{4}$ confirms this limit. Numerical examples showing that this limit is valid are presented in Example 1 of Section 5.

By manipulating (10), the following necessary condition for stability can be derived:

$$(1 - 2\mu)(1 - 2\vartheta) + 8\sigma(\mu + \vartheta - 1) \le 1. \tag{13}$$

This condition guarantees only that the highest mode is stably treated and is not sufficient for stability. Since this condition depends only on the effect of the difference operators on the highest wave number component, inequality (13) applies to any variation of the base method for which this component is treated in the same manner. In particular, this applies to any variation which uses centered differences for the normal derivative and for which the transverse derivative reverts to an upwind difference when applied to the highest wave number component. The original BCG method and each of the variations cited above fit this criteria and hence have the stability restriction (13).

The left-hand side of inequality (13) can be broken into two parts: the advective piece $(1 - 2\mu)(1 - 2\vartheta)$ and the diffusive piece $8\sigma(\mu + \vartheta - 1)$. These two functions are plotted in Fig. 3. Note that the vertical axis on the diffusive plot corresponds to units of 8σ. When μ and ϑ have values between zero and one, the advective piece has a value less than one while the diffusive piece is bounded by 8σ.

Two facts are immediately apparent from the plots. First, if $\mu \le \frac{1}{2}$ and $\vartheta \le \frac{1}{2}$, then the diffusive part is negative and inequality (13) is satisfied regardless of the size of σ. Second, if $8\sigma \ll 1$ the diffusive part will only affect the stability of the scheme for Courant numbers very close to 1. It is because of these two facts that setting the time step in the BCG method by using the advective CFL condition (11) less some small safety factor causes no stability problems in many situations.

3. A STABLE METHOD FOR INCLUDING DIFFUSIVE TERMS

The stability problems illustrated in the last section are caused by the explicit treatment of the diffusive terms

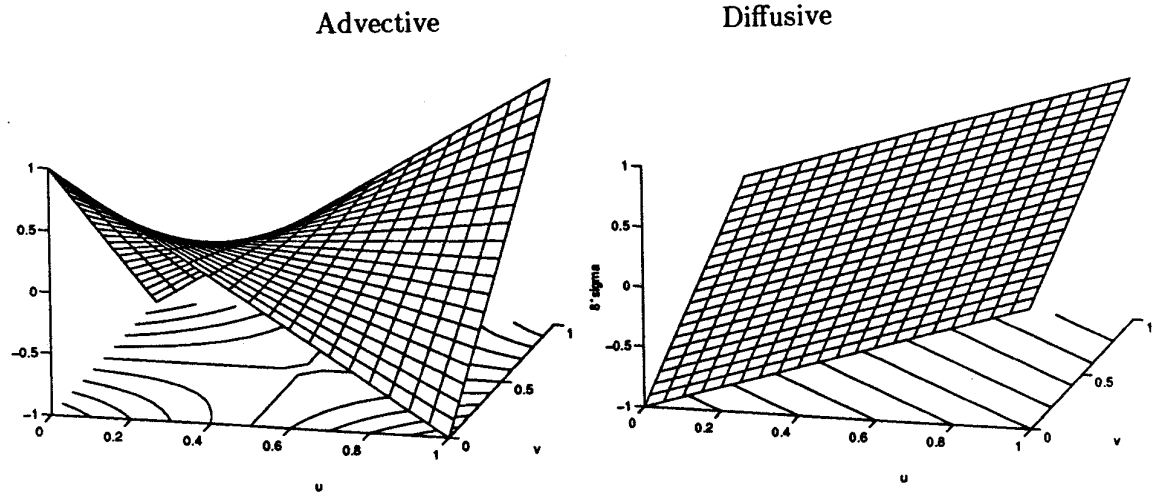

FIG. 3. The advective and diffusive parts of the stability condition. Note that the vertical axis of the diffusive part is in units of 8σ.

in the computation of time-centered cell-edge velocities. When the effect of the difference scheme on the highest wave number component is analyzed, the advective terms simplify, and the contribution of the remaining explicit diffusive terms pushes the magnitude of the symbol above 1 for $\sigma > 0$ and μ and ϑ close to 1.

It is possible, however, to remedy this problem by using a more elaborate form of the transverse derivative terms in the computation of the advective derivatives. In short, instead of computing these terms with simple upwind differences, transverse derivatives are evaluated by differencing provisional time-centered values which include diffusive terms. This procedure causes a cancellation of the contribution to the symbol and is, in effect, a diffusive or viscous extension to the method for calculating the transverse derivative terms in the original BCG method.

The form of the transverse derivatives in the original BCG method is more involved than that of the base method and is based on Colella's method for hyperbolic conservation laws [10]. Assuming again that the velocities are constant and positive, the BCG method replaces the term $D_y^-(\rho)$, appearing in Eq. (7) with a backward difference $D_y^-(\tilde{\rho})$ of the quantity

$$\tilde{\rho}_{i,j} = \rho_{i,j} + \frac{1}{2}\left(1 - \frac{\Delta t}{h} b\right) D_y^0(\rho)_{i,j}. \tag{14}$$

The remaining transverse derivative is computed in the analogous way. In the actual BCG method, the centered difference appearing in this equation is in fact a limited difference which reverts to a centered difference if no limiting is done, but again the effect of limiters is not considered here.

The necessary adjustment to the calculation of advective derivatives that yields a stable method regardless of the value of σ involves simply adding a diffusive term to the definition of $\tilde{\rho}$. Specifically, instead of the states given in (14), define the cell edge states

$$\begin{aligned}
\tilde{\rho}^T_{i,j} &= \rho^n_{i,j} + \frac{1}{2}\left(1 - \frac{\Delta t}{h} b\right) D_y^0(\rho^n)_{i,j} + \frac{\Delta t}{2}\kappa L^5(\rho^n)_{i,j}, \\
\tilde{\rho}^R_{i,j} &= \rho^n_{i,j} + \frac{1}{2}\left(1 - \frac{\Delta t}{h} a\right) D_x^0(\rho^n)_{i,j} + \frac{\Delta t}{2}\kappa L^5(\rho^n)_{i,j}.
\end{aligned} \tag{15}$$

The form of the advective derivative is now given by the convective difference (8) of the following quantities rather than those given in Eq. (7)

$$\begin{aligned}
\rho^{n+1/2,T}_{i,j} &= \rho_{i,j} + \frac{1}{2}\left(1 - \frac{\Delta t}{h} b\right) D_y^0(\rho^n)_{i,j} \\
&\quad - \frac{a\Delta t}{2h} D_x^-(\tilde{\rho}^R)_{i,j} + \frac{\kappa\Delta t}{2} L^5(\rho^n)_{i,j}, \\
\rho^{n+1/2,R}_{i,j} &= \rho^n_{i,j} + \frac{1}{2}\left(1 - \frac{\Delta t}{h} a\right) D_y^0(\rho^n)_{i,j} \\
&\quad - \frac{b\Delta t}{2h} D_y^-(\tilde{\rho}^T)_{i,j} + \frac{\kappa\Delta t}{2} L^5(\rho^n)_{i,j}.
\end{aligned} \tag{16}$$

This can be simplified to

$$\begin{aligned}
\rho^{n+1/2,T}_{i,j} &= \tilde{\rho}^T_{i,j} - \frac{a\Delta t}{2h} D_x^-(\tilde{\rho}^R)_{i,j}, \\
\rho^{n+1/2,R}_{i,j} &= \tilde{\rho}^R_{i,j} - \frac{b\Delta t}{2h} D_y^-(\tilde{\rho}^T)_{i,j}.
\end{aligned}$$

By substituting the symbol for $\tilde{\rho}$ and rearranging terms the following form of $S(\xi, \eta)$ is determined:

$$
\begin{aligned}
S(\xi,\eta) = \Bigg[& 1-\mu(1-e^{-\mathbf{i}\xi})\Big[1+\frac{1}{2}(1-\mu)\mathbf{i}\sin(\xi) \\
& -\frac{\vartheta}{2}(1-e^{-\mathbf{i}\eta})\left(1+\frac{1}{2}(1-\vartheta)\mathbf{i}\sin(\eta)\right)\Big] \\
& -\vartheta(1-e^{-\mathbf{i}\eta})\Big[1+\frac{1}{2}(1-\vartheta)\mathbf{i}\sin(\eta) \\
& -\frac{\mu}{2}(1-e^{-\mathbf{i}\xi})\left(1+\frac{1}{2}(1-\mu)\mathbf{i}\sin(\xi)\right)\Big] \\
& +\frac{\sigma}{2}\Big[1-\mu(1-e^{-\mathbf{i}\xi})\left(1-\frac{\vartheta}{2}(1-e^{-\mathbf{i}\eta})\right) \\
& -\vartheta(1-e^{-\mathbf{i}\eta})\left(1-\frac{\mu}{2}(1-e^{-\mathbf{i}\xi})\right)\Big] \\
& \times(-4+2\cos(\xi)+2\cos(\eta))\Bigg] \Bigg/ \\
& \left[1-\frac{\sigma}{2}(-4+2\cos(\xi)+2\cos(\eta))\right].
\end{aligned}
$$

The effect of $S(\xi, \eta)$ on the highest frequency mode is thus

$$
\begin{aligned}
S(\pi,\pi) = & [1-2\mu(1-\vartheta)-2\vartheta(1-\mu) \\
& -4\sigma(1-2\mu(1-\vartheta)-2\vartheta(1-\mu))]/[1+4\sigma],
\end{aligned}
$$

which can be placed in the pleasing form

$$
S(\pi,\pi) = (1-2\mu)(1-2\vartheta)\frac{1-4\sigma}{1+4\sigma}. \tag{17}
$$

The right-hand side of Eq. (17) is simply the product of the symbol for the advective terms when $\sigma = 0$ multiplied by the symbol for the Crank–Nicholson terms and has magnitude less than 1, regardless of σ, under the condition

$$
\mu \le 1 \quad \text{and} \quad \vartheta \le 1. \tag{18}
$$

Note that this is only a necessary condition for stability, but a numerical check of the full symbol for values of $\sigma = 10^n$ with n ranging from -8 to 8 gives strong evidence that the scheme is stable for all values of σ under the restriction (18). Note that these numerical checks also indicate that using fourth-order slopes, in place of the second-order slopes, for the normal derivatives does not affect the stability of the modified method. This is true also when $\sigma = 0$ (when the modified scheme and BCG are the same) as opposed to the instability of the base scheme shown in Fig. 2.

Some justification of the modification to the calculation of transverse derivatives discussed above can be provided. One can recognize $\tilde{\rho}$ as an approximation to a time-centered, cell-edge value of ρ computed by only considering the normal derivative terms in the Taylor series given in Eq. (6). The justification for differencing this quantity rather than just ρ is not at first clear since it does not improve the order of accuracy of the slope. However, using a completely different approach, LeVeque develops high-resolution methods for advection in [14]. Ignoring for a moment the implementation of slope limiters, LeVeque's methods closely match those presented here when the diffusive terms are omitted. Specifically, the algorithm in [14] referred to as Method 3 has a form identical to the base method applied to the nondiffusive linear problem. A modification to Method 3 referred to as Method 4 which includes the effect of transverse propagation of correction waves is then presented. This modification does not provide an increase in the second-order accuracy of Method 3, but it is shown to give better results. Moreover, this correction has the same form as the normal derivative terms added in Eq. (14) that differentiate the BCG method from the base method.

There is also a loose justification for the appearance of the diffusive terms in the computation of the transverse derivatives based on the derivation in LeVeque [14]. Equation (4) can be rewritten

$$
\rho_t = (-a + \kappa\partial_x)\rho_x + (-b + \kappa\partial_y)\rho_y,
$$

where ∂_x and ∂_y represent differentiation. In the derivation of Method 4 one can symbolicly replace terms of the form $a(\rho_{i,j} - \rho_{i-1,j})$ with $(a - \kappa\delta_x)(\rho_{i,j} - \rho_{i-1,j})$ and likewise terms of the form $b(\rho_{i,j} - \rho_{i,j-1})$ with $(b - \kappa\delta_y)(\rho_{i,j} - \rho_{i,j-1})$, where δ_x and δ_y are some discrete approximation to ∂_x and ∂_y. Among the additional terms that result if this substitution is carried out, are two appropriately scaled diffusive terms as in the Taylor series extrapolations in the BCG method (the Laplacian terms in the definition in Eq. (16)) and also one-dimensional diffusive terms that correspond to the terms added in the modification to the transverse derivative terms (the Laplacian terms in Eq. (15)).

Finally, it should be noted that the only additional computational expense in the modification to the BCG method involves the addition of the Laplacian term in Eq. (15). This Laplacian must be computed regardless for Eq. (16); hence, the additional computation required is insignificantly small.

4. NONLINEAR STABILITY OF AN OSCILLATING MODE

Although a Von Neumann analysis cannot be done on the full, nonlinear BCG method, it is possible to analyze the effect of the full method on a single oscillating mode.

Let

$$\omega_{i,j} = (-1)^{i+j}$$

and consider the velocity field

$$u(i,j) = 1 - \varepsilon\omega_{i,j}$$
$$v(i,j) = 1 + \varepsilon\omega_{i,j},$$

or more compactly,

$$U(i,j) = 1 \mp \varepsilon\omega_{i,j}$$

with $\varepsilon \ll 1$. Assume also that the discrete pressure is constant.

The oscillatory velocity of this example on an $N \times N$ grid is a discrete representation of the exact solution of the Navier–Stokes equations on the periodic domain $[2\pi \times 2\pi]$ given by

$$u(x,y,t) = 1 - \varepsilon\cos(N(x-t))\sin(N(y-t))e^{-2N^2\nu t}$$
$$v(x,y,t) = 1 + \varepsilon\sin(N(x-t))\cos(N(y-t))e^{-2N^2\nu t}$$
$$p(x,y,t) = -\varepsilon^2/2(\sin^2(N(x-t)) + \sin^2(N(y-t))e^{-4n^2\nu t}.$$

The velocity field here contains a divergence-free oscillatory mode that decays in time. The discrete version of this mode also has zero divergence if the divergence operator is based on a centered difference operator; hence, projections based on centered differences will not remove this mode from the numerical solution.

The effect of one time-step of the full BCG method on this velocity can easily be written down. Details of the steps of the method can be found in the references and will not be covered here. First note that any centered difference of the oscillating mode will produce a value of zero. Since $\varepsilon \ll 1$, the upwind difference operators used for transverse derivatives will at each cell be backward difference operators. In the case of the oscillating mode, the backward difference operator multiplies the mode by a factor of $2/h$. The five-point Laplacian operator simply multiplies $\omega_{i,j}$ by a factor of $-8/h^2$.

Putting these pieces together yields the following cell-edge values computed by the Taylor series extrapolations as they appear in the original BCG method (analogous to the values in Eq. (6)):

$$U_{i,j}^{n+1/2,T} = U_{i,j}^{n+1/2,B} = U_{i,j}^{n} - \frac{\Delta t}{2}(1 - \varepsilon\omega_{i,j})\left(\mp\frac{2}{h}\varepsilon\omega_{i,j}\right) + \frac{\nu\Delta t}{2}\left(-\frac{8}{h^2}\right)(\mp\varepsilon\omega_{i,j})$$

$$U_{i,j}^{n+1/2,R} = U_{i,j}^{n+1/2,L} = U_{i,j}^{n} - \frac{\Delta t}{2}(1 - \varepsilon\omega_{i,j})\left(\mp\frac{2}{h}\varepsilon\omega_{i,j}\right) + \frac{\nu\Delta t}{2}\left(-\frac{8}{h^2}\right)(\mp\varepsilon\omega_{i,j}).$$

Letting $\mu = \Delta t/h$ and $\sigma = \nu\Delta t/h^2$, after collecting terms, this becomes

$$\begin{aligned} U_{i,j}^{n+1/2,T} &= U_{i,j}^{n+1/2,B} \\ &= U_{i,j}^{n} - \mu(1 - \varepsilon\omega_{i,j})(\mp\varepsilon\omega_{i,j}) - 4\sigma(\mp\varepsilon\omega_{i,j}) \\ U_{i,j}^{n+1/2,R} &= U_{i,j}^{n+1/2,L} \\ &= U_{i,j}^{n} - \mu(1 - \varepsilon\omega_{i,j})(\mp\varepsilon\omega_{i,j}) - 4\sigma(\mp\varepsilon\omega_{i,j}) \end{aligned}$$

The upwind state at the right and top of each cell will be those given by $U_{i,j}^{n+1/2,R}$ and $U_{i,j}^{n+1/2,T}$, and using the fact that $\omega_{i,j}^2 = 1$,

$$U_{i,j}^{n+1/2,T} = 1 \mp \mu\varepsilon^2 \mp (1 - \mu - 4\sigma)\varepsilon\omega_{i,j},$$
$$U_{i,j}^{n+1/2,R} = 1 \pm \mu\varepsilon^2 \mp (1 - \mu - 4\sigma)\varepsilon\omega_{i,j}.$$

It is easy to see that the cell edge values $u_{i,j}^{n+1/2,R}$ and $v_{i,j}^{n+1/2,T}$ have a MAC-divergence of zero and, hence, are not changed by the MAC projection step first appearing in [3] and commonly applied to these edge values.

The convective form of the advective derivatives is

$$(U\cdot\nabla)U_{i,j} = (uU_x + vU_y) = \frac{(u_{i,j}^R + u_{i-1,j}^R)}{2}\frac{(U_{i,j}^R - U_{i-1,j}^R)}{h} + \frac{(v_{i,j}^T + v_{i,j-1}^T)}{2}\frac{(U_{i,j}^T - U_{i,j-1}^T)}{h},$$

and for the edge values given above yields

$$\begin{aligned} (U\cdot\nabla)U_{i,j} &= (1 + \mu\varepsilon^2)\left(\mp\frac{2}{h}(1 - \mu - 4\sigma)\right)\varepsilon\omega_{i,j} \\ &\quad + (1 + \mu\varepsilon^2)\left(\mp\frac{2}{h}(1 - \mu - 4\sigma)\right)\varepsilon\omega_{i,j} \\ &= \mp(1 + \mu\varepsilon^2)\frac{4}{h}(1 - \mu - 4\sigma)\varepsilon\omega_{i,j}. \end{aligned}$$

The full scheme in this case gives

$$\left(1 - \nu\frac{\Delta t}{2}\Delta\right)U^* = 1 \mp \varepsilon\omega_{i,j} - \Delta t\left(\mp(1+\mu\varepsilon^2)\right.$$
$$\times\frac{4}{h}(1-\mu-4\sigma)\varepsilon\omega_{i,j}$$
$$\left.+\,\nu\frac{\Delta t}{2}\Delta(1\mp\varepsilon\omega)_{i,j}\right)$$
$$= 1 \mp (1 - 4\mu(1+\mu\varepsilon^2)$$
$$\times(1-\mu-4\sigma) - 4\sigma)\varepsilon\omega_{i,j}.$$

It is easy to see that the solution to this equation is given by $U^* = 1 \mp \alpha\varepsilon\omega_{i,j}$ with

$$\alpha = (1 - 4\mu(1+\mu\varepsilon^2)(1-\mu-4\sigma) - 4\sigma)/(1+4\sigma). \tag{19}$$

This form of U^* is not changed by either the projection operator in [2] or the approximate projection in [13]; hence, for these methods $U^{n+1} = U^*$. It is exactly the fact that the oscillating mode is not affected by projection operators based on centered difference divergences that has prompted the use of filters in recent methods to remove this mode. (See the discussion in Section 6.)

In order for the oscillating part of the solution to be damped, it must be true that $|\alpha| < 1$. First, note that if $\mu = 1$,

$$\alpha = (1 + 12\sigma + 16\varepsilon^2\sigma)/(1+4\sigma).$$

This is the same condition given in Eq. (12), except for the addition of the ε^2 term. It is evident that the scheme will not damp the oscillating mode under the stability condition

$$\mu \le 1 \quad \text{and} \quad \vartheta \le 1$$

for all values of σ. Rearranging terms in (19) yields the following stability condition which is nearly the same as Eq. (13) with $\mu = \vartheta$:

$$(1-2\mu)(1-2\mu) - 4\mu^2\varepsilon^2(1-\mu)$$
$$+\,8\sigma(2\mu(1+\mu\varepsilon^2) - 1) \le 1.$$

Finally, if $\sigma = 0$, the above stability condition reduces to $\mu \le 1$, as would be expected.

The effect of the modification to the transverse derivative terms can be easily traced through this analysis and results in the time-centered edge values

$$U_{i,j}^{n+1/2,T} = 1 \mp \mu(1-4\sigma)\varepsilon^2 \mp (1 - \mu(1-4\sigma) - 4\sigma)\varepsilon\omega_{i,j},$$

$$U_{i,j}^{n+1/2,R} = 1 \pm \mu(1-4\sigma)\varepsilon^2 \mp (1 - \mu(1-4\sigma) - 4\sigma)\varepsilon\omega_{i,j}.$$

This then leads to a value of α,

$$\alpha = (1 - 4\mu(1+\mu(1-4\sigma)\varepsilon^2)(1-\mu(1-4\sigma)$$
$$-4\sigma) - 4\sigma)/(1+4\sigma)$$
$$= [(1-2\mu)(1-2\mu) - 4\mu^2\varepsilon^2(1-\mu)(1-4\sigma)]\frac{1-4\sigma}{1+4\sigma}.$$

This is the same condition as (17) with the exception of the additional ε^2 term.

Numerical experiments demonstrating the validity of the above analysis are presented in Section 5.4.

5. NUMERICAL EXPERIMENTS

In this section the results of numerical experiments will be presented that illustrate several points. First, it is shown that the stability bounds derived for the scheme without the modification presented in Section 3 do, indeed, have to be met for the method to produce stable results for the linear advection–diffusion equation. Second, two experiments are presented to illustrate that the modification to the method enables stable, second-order accurate results to be computed for problems using a wide range of σ with a CFL restriction independent of σ. Third, an experiment using the full nonlinear method will be presented that shows that the linear stability bounds are relevant in the non-linear case. Finally, results from a simulation of Boussinesq flow are included to illustrate the robustness of the algorithm when applied to a fully nonlinear system of equations.

5.1. *Instability of the BCG Method*

The first example is designed to illustrate the validity of the stability condition (13) for the advection–diffusion scheme taken from the original BCG method. In Section 2, the Von Neumann analysis given indicates that for $\sigma = \frac{1}{4}$, the stability condition is $\mu\vartheta \le \frac{1}{2}$. In order to numerically test this limit, two numerical runs are performed; one which just meets this requirement and one which just fails. The initial conditions used consist of a complicated density distribution advected by a constant velocity given by $u = v = \sqrt{2}/2$. The initial density distribution is shown in the top left picture of Fig. 4 and consists of a smooth hump, a cone, and two slotted disks of density taken from [14].

For each run, the advective CFL condition

$$\Delta t = C\frac{h}{\max\limits_{i,j}(|u_{i,j}|, |v_{i,j}|)} \tag{20}$$

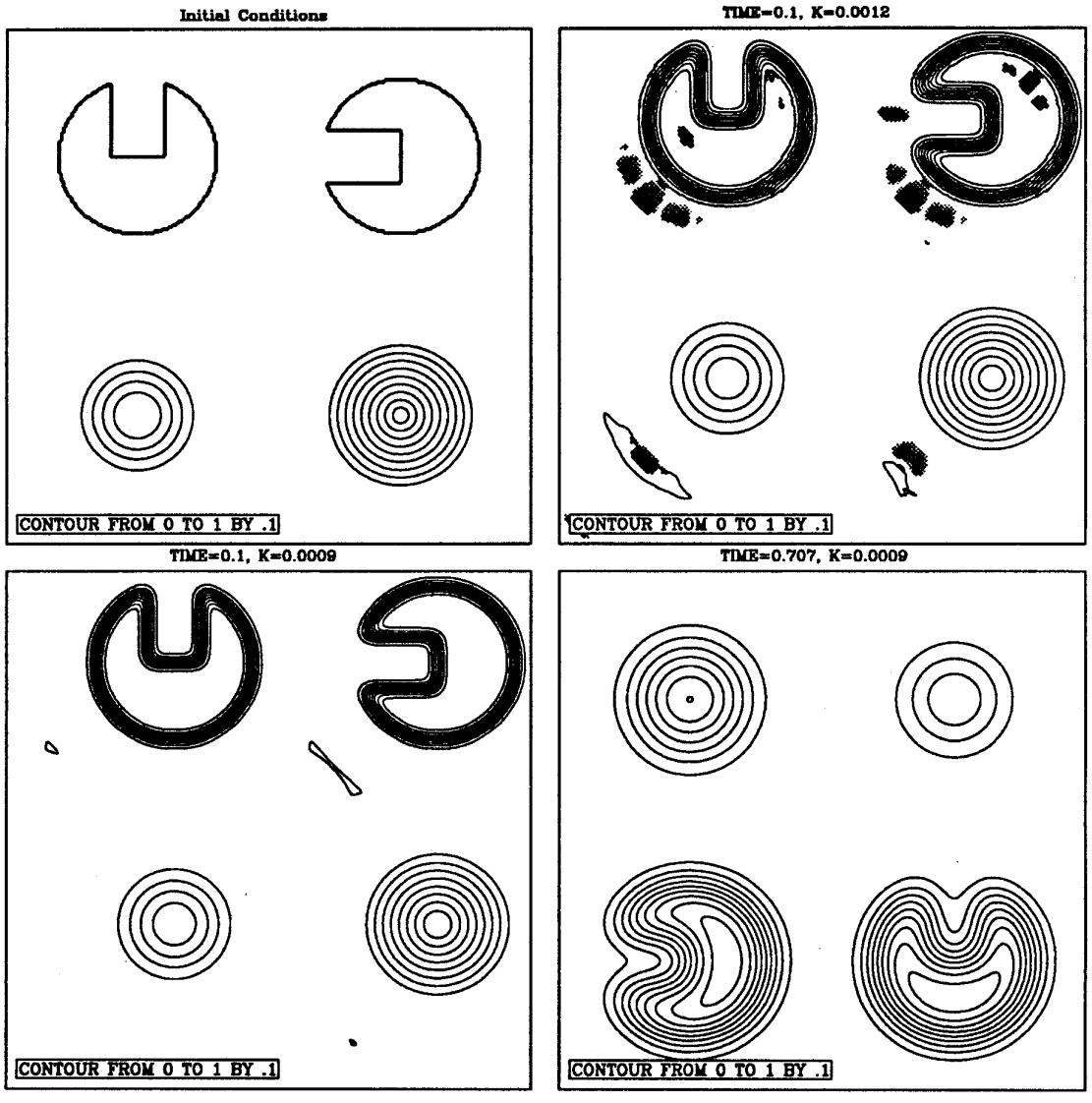

FIG. 4. Contour plots of the density from example 5.1.

is used to set the time step where C is the advective CFL number, $C = \sqrt{2}/2$. Since $u = v = \sqrt{2}/2$, this corresponds to setting $\mu = \vartheta = \sqrt{2}/2$ and $\Delta t = h$. A 256×256 grid is used ($h = \frac{1}{256}$) which gives a value of $\sigma = 256\kappa$. Hence, if the Von Neumann analysis is valid, the scheme should be stable when $\kappa < \frac{1}{1024}$ and unstable when $\kappa > \frac{1}{1024}$. Figure 4 shows the results from the two experiments. The top right picture shows a contour plot of the density after time $t = 0.1$ computed with $\kappa = 0.0012$ in which oscillations at the trailing edge of density jumps are clearly evident. These oscillations continue to grow exponentially during the calculation. The bottom two pictures show the density at time $t = 0.1$ and $t = \sqrt{2}/2$ computed with $\kappa = 0.0009$ and illustrate that at this value, stable results are being computed.

5.2. *Stability of the Modified BCG Method*

To illustrate the stability of the BCG method with the modification of the transverse derivatives, the same problem as above is run with $\kappa = 0, 0.0001, 0.001$, and 0.01. Figure 5 shows the density contours at time $t = \sqrt{2}/2$ for each value of κ computed on a 256×256 grid with the advective CFL number $C = 0.95$. This corresponds to values of σ ranging from 0 to approximately 3.44. It is evident from the figures that the modified method is stably computing the solution for each value of κ.

5.3. *Convergence of the Modified Method*

To illustrate the accuracy of the modified BCG method when applied to the advection–diffusion equation, the ad-

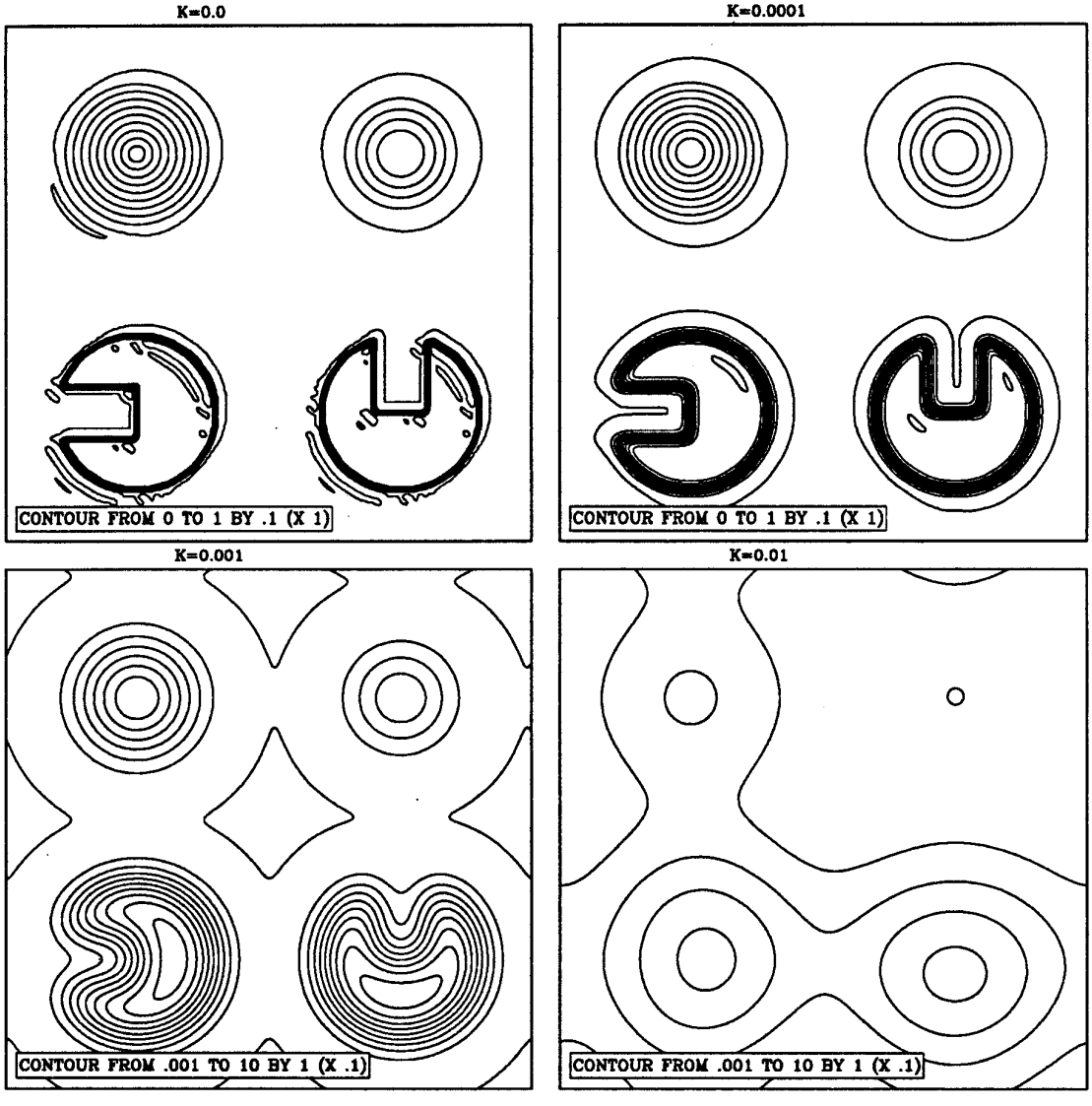

FIG. 5. Contour plots of the density from example 5.2.

vection of a Gaussian initial density

$$\rho(x, y, 0) = \frac{1}{4\pi\kappa}\exp\left(\frac{-r^2}{4\kappa}\right),$$
$$r^2 = (x - 0.5)^2 + (y - 0.5)^2,$$

is computed. A constant flow given by $u = 10.0$ and $v = 5.0$ is used, and the domain is a doubly-periodic unit square. The initial conditions can be thought of as an infinite lattice of Gaussians being advected by a constant flow and diffusing at a rate governed by the magnitude of κ. For larger values of κ the contributions to the solution from nearby lattice sites must be considered when computing the exact solution. After time $t = 0.2$, the exact solution for a single Gaussian when $\kappa > 0$ is given by

$$\rho(x, y, 0.2) = \frac{1}{4\pi\kappa 1.2}\exp\left(\frac{-r^2}{4\kappa 1.2}\right).$$

When $\kappa = 0$, the solution at time $t = 0.2$ is the same as the initial conditions.

Solutions are computed on three different grids with 64, 128, and 256 grid points in each dimension, respectively. Four runs are performed for each grid size corresponding to $\kappa = 0, 0.001, 0.01$, and 0.1. A CFL number of $C = 0.9375$ is used for all runs which correspond to $\mu = 0.9375$ and $\vartheta = 0.46875$. Values of σ range from 0 to 24. For each case the $L1$ norm of the error of the numerical solution is computed and is listed in Table I in the columns labeled "64" etc. The convergence rates are computed by taking the $\log_2$ of the ratio of errors on successive grids and are given under the

TABLE I

Convergence Rates of the Method for the Advected Gaussian Problem

κ	64	Rate	128	Rate	256
0.0	2.58E-1	1.80	7.40E-2	1.99	1.86E-2
0.001	2.02E-1	1.91	5.42E-2	2.05	1.31E-2
0.01	6.60E-3	2.01	1.63E-3	2.00	4.09E-4
0.1	1.19E-5	1.84	3.32E-6	1.92	8.77E-7

headings "rate." A log–log graph of the errors is also provided in Fig. 6. It is evident from the data that not only is the method computing stable results for this problem with a stability condition that does not depend on the size of κ, but it is also converging to the exact solution at a second-order rate.

5.4. *Stability of the Nonlinear Method*

In this example, the full nonlinear BCG method and the modification thereof are applied to a velocity field consisting of the sum of a constant field and a highly oscillatory mode. It is shown that the size of the oscillatory mode grows when the original BCG method is used, but it is quickly damped when the modification is employed. Moreover, nearly exact agreement with a rate of growth predicted by an analysis in Section 4 will be shown. The relevance of this problem is discussed in Section 6.

Consider the evolution of the discrete velocity

$$U(i, j) = 1 \mp \varepsilon(-1)^{i+j}$$

by Eq. 2 computed on a periodic domain. The density here is constant, $\gamma = 0.0$, and it is assumed that $\varepsilon \ll 1$. The analysis appearing in Section 4 predicts that the numerical solution at time step n for this problem given by the BCG method will be

$$U^n(i, j) = 1 \mp \alpha^n \varepsilon(-1)^{i+j}, \tag{21}$$

where α depends on ε, $\mu = \Delta t/h$, and $\sigma = \nu\Delta t/h^2$.

Numerical experiments using the original BCG method and the modified version on the oscillatory velocity field were performed on a 128×128 grid with $\varepsilon = 0.001$, $\mu = 0.9$, and $\nu = 0.001$. The analysis in Section 4 predicts the value for α for the original BCG method is approximately 1.2583 which means, of course, that the oscillations will grow in time at an exponential rate. The same analysis gives $\alpha \approx 0.23623$ for the modified method. The plots in Fig. 7 show the relative difference between the maximum value of the velocity taken from the numerical runs and the predicted values from Eq. (21) with the values of α just mentioned. In both cases the agreement is very good.

5.5. *A Boussinesq Flow Simulation*

To illustrate the robustness of the modified BCG method when applied to the full Boussinesq approximation, Eq.

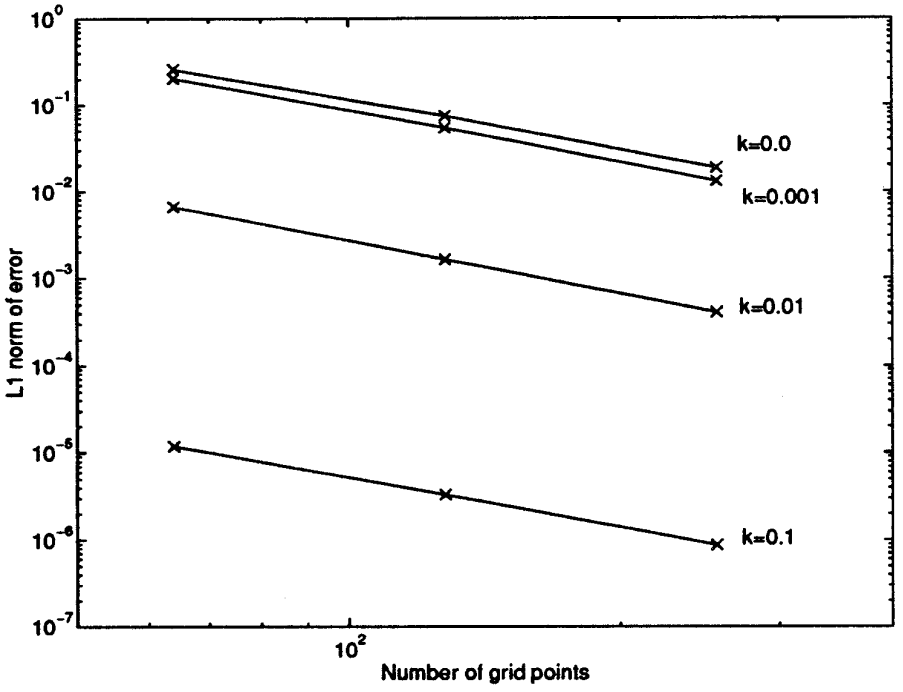

FIG. 6. Log–log plot of errors from advected Gaussian runs of example 5.3.

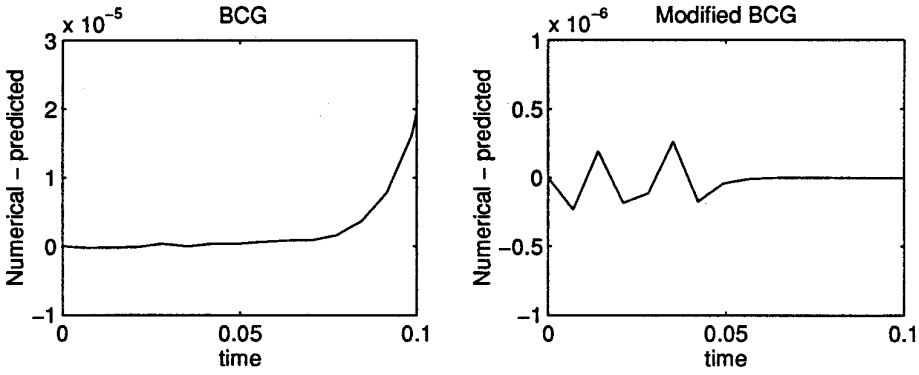

FIG. 7. Relative difference between maximum of velocity and predicted value from example 5.4.

(2) is solved on a periodic 256×256 grid with initial velocity given on the unit square by the unperturbed shear flow

$$u(x, y) = 0.0,$$

$$v(x, y) = \begin{cases} \tanh((x - 0.25)/\delta) & \text{for } x \le 0.5, \\ \tanh((0.75 - x)/\delta) & \text{for } x > 0.5, \end{cases}$$

with $\delta = 0.03$. The initial density, taken from [11], has the form of a flattened bubble and is given by

$$\rho(x, y) = 100\rho_1(x, y)\rho_2(x, y)[1 - \rho_1(x, y)],$$

where

$$\rho_1(x, y) = \begin{cases} \exp(1 - d^2/(d^2 - r^2)), \\ \qquad \text{if } (y - 0.25)^2 + (x - 0.5)^2 = r^2 < d^2 \\ 0, \qquad \text{else} \end{cases}$$

and

$$\rho_2(x, y) = \begin{cases} \exp(1 - c^2/(c^2 - (y - 1.25)^2)), & \text{if } |y - 1.25| < c, \\ 0, & \text{if } |y - 1.25| \ge c, \end{cases}$$

with $c = 0.975$ and $d = 0.25$. For this run, the viscosity ν and diffusivity κ are both 10^{-4}, and the gravitational constant $\gamma = 1$.

The numerical scheme used for this problem is adapted from the one in [15] with the modification to the advective derivatives presented here, coupled with the method for the density equation from [4] (again with the modification to the advective derivative terms). No slope limiters of any kind are used in this calculation, and the time step is computed each step to be at the limit of the linear stability bound, i.e., Eq. (20) is used with $C = 1$.

The numerical results are displayed in Figs. 8 and 9. In each frame of these two figures, a contour plot is displayed the right side of which shows the density field and the left side the vorticity (the solution is symmetric about the center line). Both the density and vorticity are scaled in these plots to have values between 0 and 1, and the contour levels range from 0.02 to 0.98 in increments of 0.12. Also, in order to suppress nonrelevant noise in the contour line corresponding to zero vorticity, any value of the scaled vorticity within 10^{-4} of 0.5 is plotted as having value 0.5.

The dynamics illustrated in these plots are quite complicated. Initially, the density bubble is situated between two strong shear layers. As the bubble begins to rise, the resulting perturbation to the velocity field causes the shear layers to become unstable and roll up into two counterrotating vortical structures. Later in the calculation, the bubble is dramatically stretched as it passes between the vortical centers, and the tails of the bubble eventually wrap around these rotating structures.

6. CONCLUSIONS

A simple, computationally inexpensive modification to the Godunov procedure for computing the time-centered advective derivatives in the method of Bell, Colella, and Glaz has been presented. It has been shown that, with this modification, the method has a stability restriction which does not depend on the diffusive coefficient for the linear advection–diffusion equation. Since the extra computational effort required for this modification is negligible, it should be utilized in the computation of all advective derivatives in coupled systems. With the modification, the BCG scheme effectively reaches one of its primary design criteria: to produce stable results for arbitrary initial data, regardless of the cell Reynolds number.

The analysis given in Section 4 suggests that the modifi-

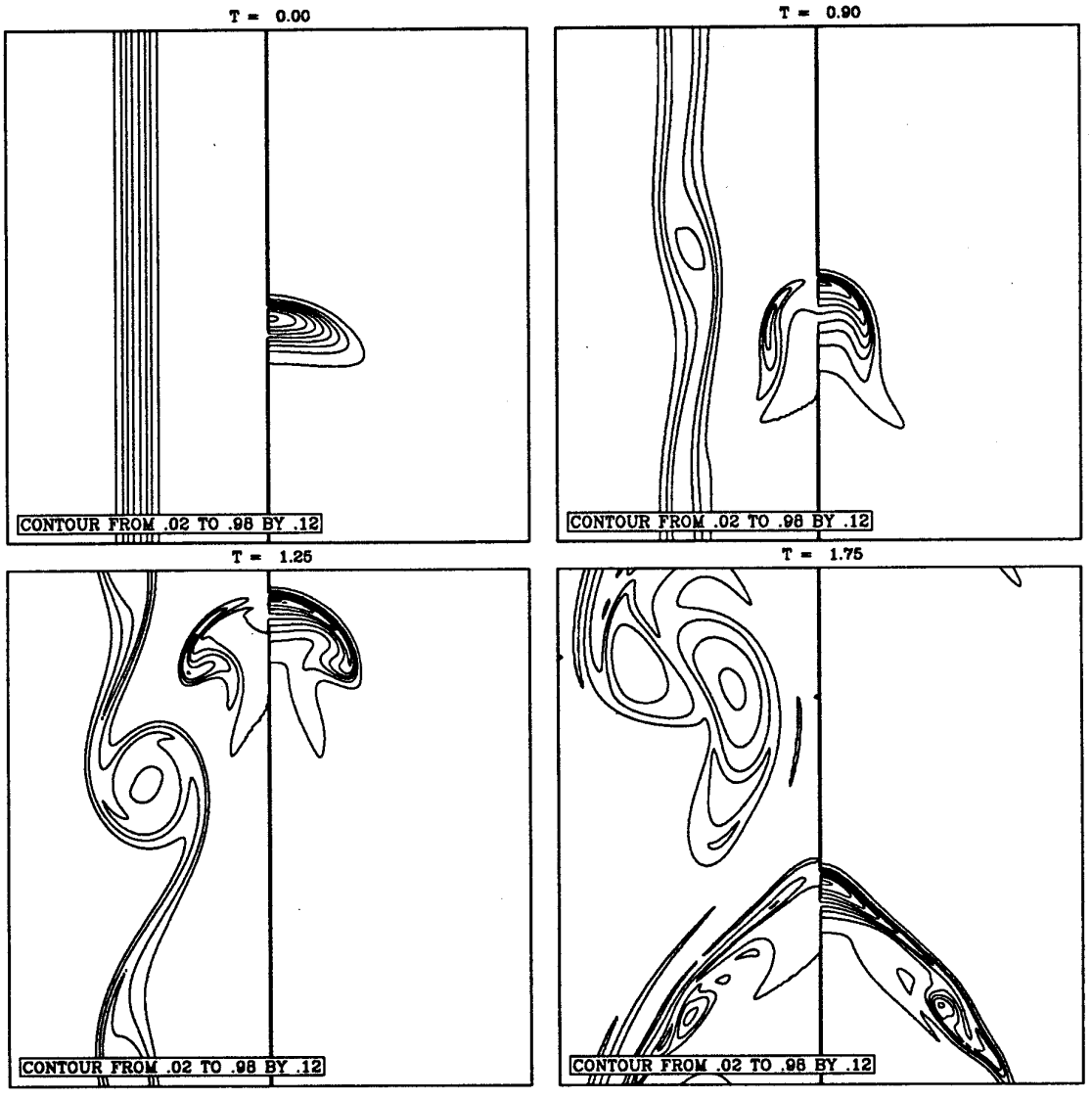

FIG. 8. Contour plots from example 5.5. In each plot, the scaled vorticity is on the left and the scaled density on the right.

cation applied to the full nonlinear method enables the method to strongly damp oscillatory modes in the velocity that persisted or grew when computed with the original method. This analysis is confirmed by the example in Section 5.4 and has particular relevance in light of recently proposed approximate projection methods.

In recent works it is argued that such oscillatory modes are not physically reasonable and, hence, should be removed from the flow [17, 13]. In order to achieve this, velocity "filters" are developed to damp oscillatory modes from the numerical solutions and improve results. In the method for reacting flows in [13], an additional and similar filter is applied to the mass fraction field. The numerical experiments presented in these works suggest that such oscillations can be introduced into the numerical solutions by source terms from reacting flows and/or the interaction of variable density approximate projections with large discontinuous jumps in the density. Example 5.4 illustrates that once introduced, BCG type methods will not damp such modes in the absence of viscosity and even worse, can accelerate their growth in the presence of even a small amount of viscosity. It is important to note also that slope limiters commonly used for the advective derivative in BCG type schemes have no effect on the analysis in Section 4 and, hence, will not help avoid this type of instability.

If the numerical solution is faithfully representing the physical system, however, in the presence of viscosity these modes should be damped, and the modification to the BCG method appears to do just that. The modification is, of course, not relevant to simulations in which no physical

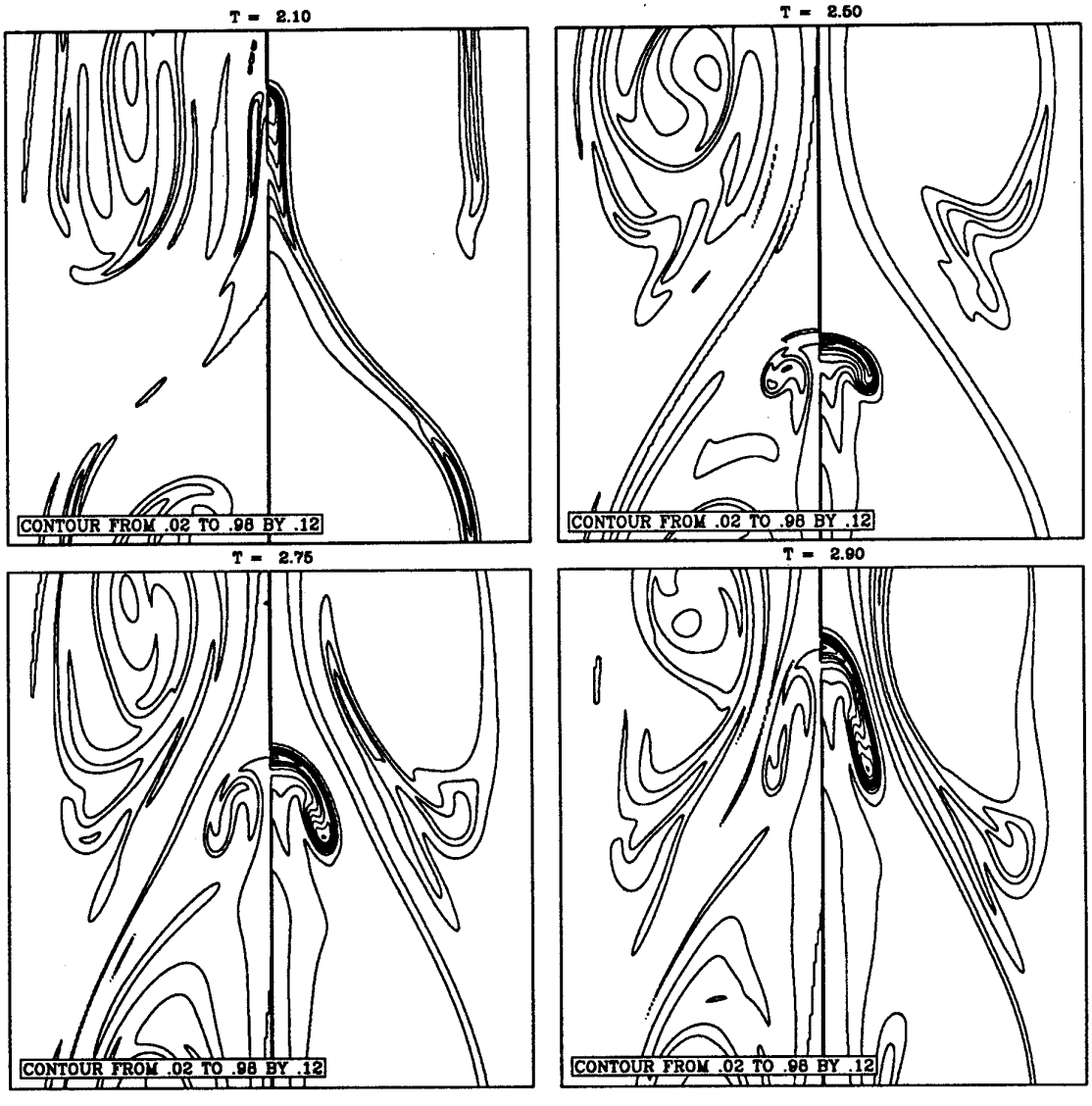

FIG. 9. Contour plots from example 5.5. In each plot, the scaled vorticity is on the left and the scaled density on the right.

viscosity is prescribed, but it is logical that the use of the modification to the BCG method presented here may help reduce or eliminate the necessity for filters in simulations where viscosity is present.

The example in Section 5.5 illustrates one final point. There is little doubt that by the end of this numerical run, the solution is being underresolved in some parts of the flow. However, because of the stability of the method, the solution remains smooth, even without slope limiting, and the basic structure of the shear layer and bubble can be seen. There can, however, be substantial differences between underresolved and fully resolved calculations, some of which are studied in [5], and the results of underresolved flows must be viewed with caution. (Incidentally, the modification to the BCG method developed in this work appears to have no effect on the results contained in [5].)

REFERENCES

1. A. S. Almgren, J. B. Bell, P. Colella, and L. H. Howell, "An Adaptive Projection Method for the Incompressible Euler Equations," in *Proceedings, Eleventh AIAA Computational Fluid Dynamics Conference, June 1993,* p. 530.
2. J. B. Bell, P. Colella, and H. M. Glaz, *J. Comput. Phys.* **85**(2), 257 (1989).
3. J. B. Bell, P. Colella, and L. H. Howell, "An Efficient Second-Order Projection Method for Viscous Incompressible Flow," in *Proceedings, Tenth AIAA Computational Fluid Dynamics Conference, June 1991,* p. 360.
4. J. B. Bell and D. L. Marcus, *J. Comput. Phys.* **101**(1), 1 (1992).

5. D. L. Brown and M. Minion, Report LA-UR-94-9999, Los Alamos National Laboratory, 1994 (unpublished).
6. S. Chandrasekhar, *Hydrodynamic and Hydromagnetic Stability* (Clarendon Press, London, 1961).
7. A. J. Chorin, *Stud. Numer. Anal.* **2,** 64 (1968).
8. A. J. Chorin, *Math. Comput.* **22,** 742 (1968).
9. A. J. Chorin, *Math. Comput.* **23,** 341 (1969).
10. P. Colella, *J. Comput. Phys.* **87,** 171 (1990).
11. W. E. and C. W. Shu, *J. Comput. Phys.* **110,** 39 (1994).
12. P. M. Gresho and R. L. Sani, *Int. J. Numer. Methods Fluids* **7,** 1111 (1987).
13. M. F. Lai, Ph.D. thesis, University of California, Berkeley, 1993 (unpublished).
14. R. J. LeVeque, Technical report, Department of Mathematics and Applied Mathematics, University of Washington, 1993 (unpublished).
15. M. Minion, Ph.D. thesis, University of California, Berkeley, 1994 (unpublished).
16. R. Peyret and T. D. Taylor, *Computational Methods for Fluid Flow* (Springer-Verlag, New York, 1983).
17. W. J. Rider, Report LA-UR-94-2000, Los Alamos National Laboratory, 1994 (unpublished).
18. J. C. Simo and F. Armero, *Comput. Methods Appl. Mech. Eng.* **111,** 111 (1994).
19. B. Van Leer, *J. Comput. Phys.* **23,** 276 (1977).